ELSEVIER

Seminars in
ULTRASOUND
CT and MRI

Pearls and Pitfalls of Metabolic Liver Magnetic Resonance Imaging in the Pediatric Population

Amirkasra Mojtahed, MD,* Michael S. Gee, MD, PhD,* and Takeshi Yokoo, MD, PhD†

Recent advances in magnetic resonance imaging (MRI) technology have moved imaging beyond anatomical assessment to characterization of tissue composition. There are now clinically validated MRI-based quantitative techniques for assessing liver fat, iron, and fibrosis, and MRI is now routinely used in metabolic liver disease evaluation in both pediatric and adult patients. These MRI techniques provide noninvasive quantitation of liver metabolic biomarkers that are increasingly relied upon in the clinical management of pediatric patients with nonalcoholic fatty liver disease, metabolic syndrome, and hemochromatosis and/or hemosiderosis. This article provides a review of the clinical indications and technical parameters for performing metabolic liver MRI in the pediatric population, along with common pearls and pitfalls encountered during its performance.
Semin Ultrasound CT MRI 41:451-461

Introduction

Metabolic liver disease encompasses several genetic and acquired chronic liver diseases that result in the abnormal accumulation of elements and metabolites within the liver. Magnetic resonance imaging (MRI) plays a pivotal role in the management of these patients by providing noninvasive quantitative assessment of these elements and metabolites that can be used as a biomarker of disease severity as well as response to treatment. The use of MRI in the assessment of metabolic liver disease is typically a 3-part approach with measurements of hepatic fat and iron concentration, as well as measurement of liver stiffness as a surrogate biomarker of hepatic fibrosis.

In the pediatric population, there are 2 main indications for metabolic liver MRI: nonalcoholic fatty liver disease (NAFLD) and iron overload. NAFLD is the most common chronic liver disease in children and is characterized by hepatic steatosis.[1] The hepatic iron overload population includes dysmetabolic iron overload syndrome, the genetic condition hemochromatosis and the acquired condition hemosiderosis. The long-standing accumulation of fat and/or iron in the liver activates inflammatory pathways leading to hepatitis that, if left untreated, ultimately progress to fibrosis and cirrhosis with concomitant risk of liver failure and hepatocellular carcinoma. Elevated liver fat has been associated with the metabolic syndrome, which is a clustered condition of obesity, dyslipidemia, hypertension, and insulin resistance.[2] In both children and adults, the metabolic syndrome confers an increased risk of diabetes and cardiovascular disease.[3,4] Hepatic steatosis alone has been shown to be an independent risk factor for developing type 2 diabetes mellitus and hypertension with the subsequent associated cardiovascular morbidity and mortality.[5,6] Hepatic iron is considered a reliable indicator of total body iron stores[7] with elevated hepatic iron concentration also conferring risk of diabetic and cardiac dysfunction through iron toxicity in the pancreatic beta cells and myocardium, respectively.[8-10] MRI provides a noninvasive method to quantify the hepatic concentrations of fat and iron, providing an objective assessment of disease severity and an imaging biomarker of patient response to therapy. The ability to assess hepatic steatosis provides an endpoint for lifestyle and dietary modifications as well as pharmacotherapy.[11-13] Liver iron quantification is helpful to guide therapeutic phlebotomy in the setting of hemochromatosis or iron chelation therapy in hemosiderosis (particularly important given the potential risk of hearing impairment from chelator therapy).[14-16] In addition, the ability to measure the degree of hepatic fibrosis provides valuable actionable prognostic information, since fibrosis confers an elevated risk of long-term hepatic and extrahepatic (endocrine and/or cardiac) complications and provides

*Department of Radiology, Massachusetts General Hospital, Harvard Medical School, Boston, MA.
†Department of Radiology, University of Texas Southwestern School of Medicine, Dallas, TX.
Address reprint requests to Michael S. Gee, MD, PhD. Division of Pediatric Radiology, Massachusetts General Hospital, 55 Fruit St., Ellison 237, Boston, MA 02114. E-mail: msgee@mgh.harvard.edu

https://doi.org/10.1053/j.sult.2020.05.010
0887-2171/

an indication for aggressive therapeutic intervention, including the potential use of anti-fibrotic agents that are entering clinical practice in certain settings.[17-19]

Historically, liver biopsy has been the gold standard for the grading of hepatic steatosis, iron concentration and staging of fibrosis. However, MRI has key advantages over biopsy in routine clinical practice. Histologic assessment of liver fat, iron and fibrosis is performed on a visual scale by a human reader and is inherently subjective and prone to intra- and/or inter-reader variabilities. By providing a quantitative assessment, MRI is more objective and less prone to the intra- and/or inter-reader variabilities.[20,21] Furthermore, these disease processes are also heterogeneous within the liver and MRI, by providing whole liver assessment, is not susceptible to sampling bias associated with standard liver biopsy that only assesses approximately 1 of 50,000th of the liver volume.[22] Finally, liver biopsy is invasive, expensive, and associated with a small but nonzero risk of complications,[23-26] while MRI is noninvasive, less expensive, and preferred by patients and referring clinicians alike. Also, in the pediatric population liver biopsy often requires deep sedation or general anesthesia, which is associated with its own risks and increases procedure time and financial cost. Patients with metabolic liver disease undergo multiple assessments over time to evaluate treatment efficacy and disease progression, and minimizing the risks associated with repeated invasive procedures is ideal.

Metabolic Liver MRI Techniques

The key components of a metabolic liver disease MRI protocol are a proton density fat-fraction (PDFF) map to measure steatosis, an R2* map to measure iron, and an elastography stiffness map to measure fibrosis. The PDFF and R2* can be measured simultaneously in a single pulse sequence. These methods are currently done using breath-hold acquisitions, but free breathing acquisitions are either recently available or in clinical development (described below), which would be particularly useful for neonates and young children unable to follow breath hold instructions. MR elastography techniques are currently only available for breath-hold acquisitions. Liver stiffness value is not biased by steatosis or iron per se, though the technical success rate may be affected by degree of iron overload as explained later.

Hepatic Fat Quantification

Hepatic steatosis is a hallmark of NAFLD and on a cellular level represents the accumulation of triglyceride-containing vesicles within hepatocytes.[27-29] On MRI, the degree of steatosis is quantitated as PDFF. This is the fractional concentration of protons (^{1}H) belonging to the triglyceride molecule and is the standardized chemical measure of tissue triglycerides. PDFF is typically obtained in clinical practice by chemical shift-encoded imaging using a multiecho spoiled gradient recalled echo (GRE) sequence, also referred to as multiecho Dixon imaging. Chemical shift-encoded imaging leverages a priori known difference in precessional frequencies of the triglyceride and water protons. Fat quantity measured by multiecho Dixon imaging is more accurate than that measured by traditional T1-weighted dual-echo Dixon imaging (in- and opposed-phase imaging), by correcting for confounders including T1 bias, T2* decay and the spectral complexity of fat. T1 bias refers to the overestimation of fat quantity by T1-weighted sequences due to the shorter T1 of the triglyceride protons (eg, ~200 at 1.5T) compared to longer T1 of the water protons in the liver (~570 at 1.5T).[30-32] Multiecho Dixon techniques can use sufficiently low flip angles to minimize T1-weighting, such that this T1 bias of fat vs water signal becomes negligible. Individual differences in liver T2*, which can vary from normal (>16s at 1.5T) to quite short (<2s at 1.5T) in patients with severe iron overload,[33] can confound fat quantification because both fat and the T2* decay contribute to the MR signal differences across multiple echo times. To obtain accurate fat quantity irrespective of hepatic iron loading, T2* correction is necessary.[34] This correction is also the basis of hepatic iron concentration measurement described later in this paper. Finally, the triglyceride molecule has multiple spectral peaks of different precession frequencies corresponding to various proton-containing chemical moieties.[35] Traditional in- and opposed-phase imaging only accounts for the dominant peak relating to the methylene (-CH2-) component and results in errors. At multiecho Dixon imaging, the multiple fat peaks can be incorporated in the fat quantification based on their known relative concentrations in a process called multipeak reconstruction.[36] If and only if these confounders of MR signals are corrected, the fat quantity measured by multiecho Dixon becomes a proton-based chemical metric, or PDFF. PDFF by multiecho Dixon has been shown to be an accurate and reproducible imaging biomarker for the assessment of hepatic steatosis in children with NAFLD.[37,38]

Sequence and Parameters

PDFF mapping can be performed using a multiecho 2D or 3D GRE sequence. The specific parameters used to create PDFF maps vary among vendors and field strengths. Example parameters on a 1.5T system are listed in Table 1. This technique typically allows for mapping of the entire liver in a single breath-hold.

MR spectroscopy was traditionally used for noninvasive hepatic fat quantification prior to the advent of PDFF imaging techniques, because of its ability to specifically measure each of the multiple spectral peaks of the triglyceride molecule.[39-43] However, multiple studies subsequently showed that PDFF measured by MR imaging is equivalent to that by MR spectroscopy.[44-47] The inherent restriction of spatial coverage with single or multivoxel MR spectroscopy limits its utility in longitudinal assessments given the heterogeneity of hepatic steatosis. MR spectroscopy is also time and resource intensive, further limiting its widespread applicability. Some vendor-specific platforms for metabolic liver MRI (eg, LiverLab; Siemens Healthineers, Malvern, Pennsylvania) include single voxel MR spectroscopy as a reference value for the PDFF map by imaging.

Table 1 Example Sequence Parameters for a Combination Proton Density Fat-Fraction (PDFF)/R2* GRE Pulse Sequence on a 1.5T Clinical MR Scanner

	PDFF/R2*
Matrix	256 × 64
NEX	1
First TE (ms)	2.3
Delta TE (ms)	2.3
Total number of echoes	6
TR (ms)	≥ 120
Bandwidth	≥ 500
Flip angle	25
Slice thickness (mm/gap)	8/0
Scan time	One ~15 sec breath-hold

Interpretation Pearls

PDFF maps are simple to interpret. Regions of interest (ROI) are placed on the liver and the corresponding values represent the mean PDFF value, reported as a percentage ranging from 0% (no fat) to 100% (all fat). Subcutaneous and visceral fat typically have values close to 100%, and lean organs such as the spleen have ~0%. Different approaches to liver ROI placement exist, but the main principle is to report a value, or a range of values when steatosis is heterogeneous, which represents the overall level of steatosis in the liver. Although there is no consensus recommendation on how ROIs should be placed, the most reproducible method is to sample as much of the liver as possible by averaging large ROIs and taking care to avoid major vessels (Fig. 1A).[48] The ROIs may be circular or free-form in shape. Depending on the MR and Picture Archiving and Communication System (PACS) vendors, the PDFF map may be sent through to PACS, allowing the radiologist interpreting the study to redraw ROIs later. If not, then the ROIs will need to be drawn at the MRI console or on an offline workstation and then sent through to PACS for interpretation and reporting.

Pitfalls

The multiecho GRE sequence used to create the PDFF maps is traditionally run using a single breath-hold which provides sufficient coverage to image the entire liver. Breath-hold imaging can pose a challenge in the pediatric population and care should be taken to recognize motion artifacts and place ROIs in areas that are spared from motion. For younger children, breath hold exercises with a technologist or child life specialist before the exam can help improve breath hold duration and image quality.[49] Newer techniques are emerging to allow for free-breathing assessment, including variant pulse sequences using radial K-space filling rather than traditional Cartesian ordering, as well as respiratory gating.[50] Radial sampling offers the advantage of dispersing respiratory phase-encoding artifacts across the entire imaging plane (2D) or volume (3D), and also is associated with oversampling of the center of K-space that is the primary contributor to image contrast.[51] This allows for relatively motion-robust metabolic liver evaluation in patients without the requirement for respiratory suspension.[52,53]

The chemical shift-based fat-water separation technique that is the basis of PDFF is susceptible to an artifact called "fat-water swap" or "pixel swap." This artifact is specific to Dixon fat-water separation techniques and occurs as the result of a phase error during the computational step required to separate the signal contributions of fat and water. The artifact manifests as a swapping of the pixel values on the corresponding fat and water maps (ie, assigning a value for fat where it should be water, and vice-versa). This may happen in a geographic manner in parts of the imaging volume or in the entire imaging volume (Fig. 2). The cause may be related to the presence of susceptibility in the field or incomplete shimming of B_0 inhomogeneity, but in some instances no known cause may be identifiable. Repeating the sequence or re-shimming using smaller shim volume may be helpful, particularly if the cause is identifiable and can be addressed. Another less frequent cause of PDFF mapping failure is in the setting of severe iron overload, which will be discussed in the next section.

Hepatic Iron Quantification

Elevated serum ferritin is a frequent finding in patients with NAFLD, insulin resistance, and other features of metabolic syndrome.[54-57] While ferritin can be elevated in an inflammatory state alone (as it is an acute phase reactant) including

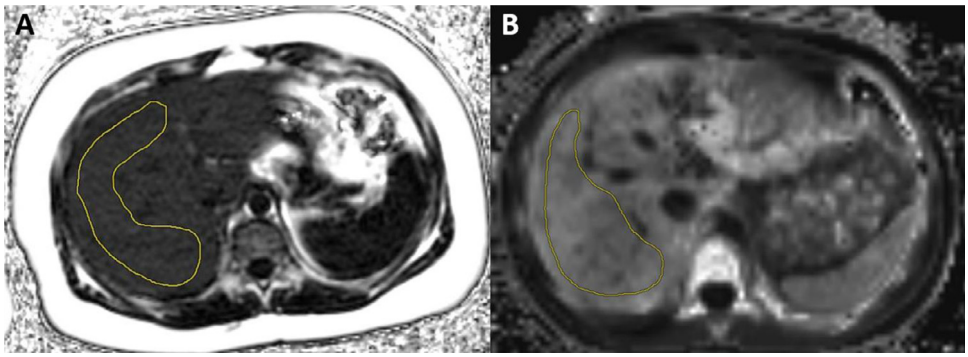

Figure 1 Representative proton density fat-fraction map (A) of a 12-year-old male with NAFLD and R2* map (B) of an 8-year-old male with sickle cell anemia showing acceptable ROI placement.

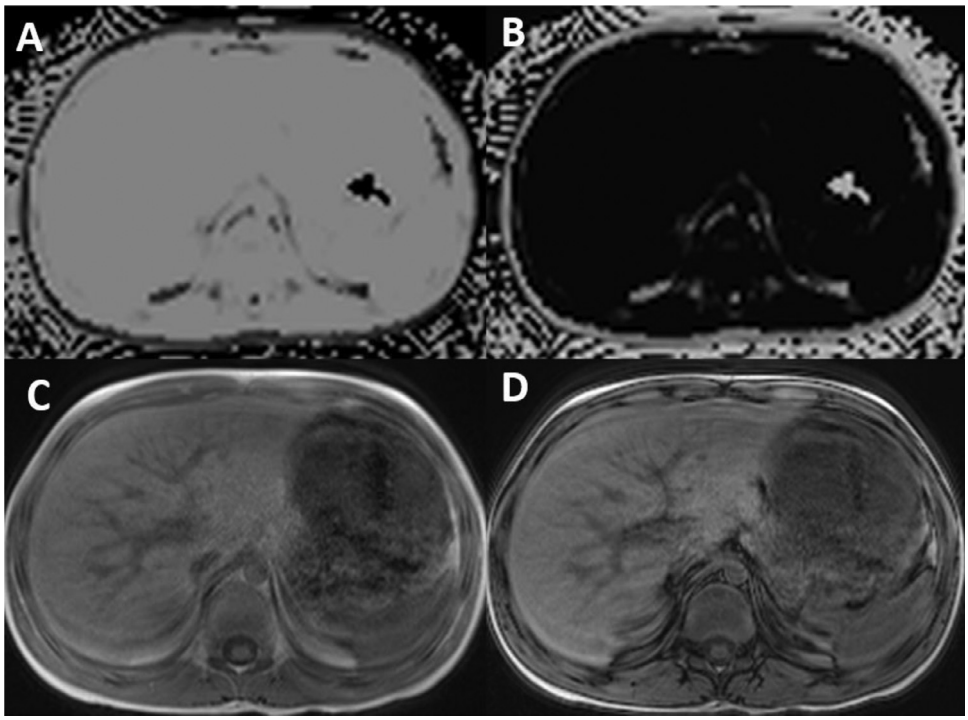

Figure 2 Metabolic liver MRI images for a 10-year-old male with hyperferritinemia demonstrate fat-water swap on the proton density fat-fraction (A) and water (B) images. The in-phase (C) and opposed-phase (D) images are provided for reference demonstrating no significant signal loss.

steatohepatitis, parenchymal iron accumulation can develop in the absence of hepatocellular inflammation.[58] This condition called dysmetabolic iron overload syndrome, is believed to be caused by aberrant iron homeostasis, and may be implicated in the development or exacerbation of insulin resistance, atherosclerosis, and hepatocellular toxicity.[59] While the degree of iron overload is usually mild in dysmetabolic iron overload syndrome, more severe liver iron overload can develop in patients from nonmetabolic causes, such as hereditary hemochromatosis and transfusional iron overload. Serious complications of hereditary hemochromatosis are rare in childhood as clinically significant iron loading does not occur until adulthood. The most common cause of severe iron overload in childhood is transfusional. Transfusional iron overload occurs in many primary and secondary anemias including thalassemias, sickle cell disease, aplastic anemia, leukemia, and other hematologic malignancies for which repeated red blood cell transfusions are required. Traditional serum laboratory values such as serum ferritin correlate poorly with liver iron stores as they are acute phase reactants that can fluctuate over time depending due to a variety of inflammatory states,[60] including steatohepatitis. Therefore, direct measurement of liver iron concentration is needed. MRI represents an ideal method to measure the liver iron concentration, estimate the risks of hepatoxicity, and serve as a prognostic biomarker for the systemic toxicity of iron overload conditions.

Multiple MRI-based methods can be used to measure the liver iron concentration, including R2* relaxometry, R2 relaxometry or the signal-intensity ratio method.[33] In the United States, R2* and R2 relaxometry are most commonly used. The R2 relaxometry method is well established and FDA approved, but has several drawbacks compared to the R2* method. R2 relaxometry uses multiple free-breathing acquisitions of a single spin echo sequence at different echo time (TEs). As the result, the exam has a long acquisition time (~15 minutes), is limited to several (typically ~11) slice coverage, and prone to motion artifacts which can be severe. In addition, R2 relaxometry is currently a commercial product that requires transfer of MR images to an external site for analysis (FerriScan; Resonance Health, Burswood, Australia), which delays turnaround time and adds additional cost not currently covered by most health insurance carriers in the United States. Given these limitations, many centers have moved towards R2* relaxometry which in contrast to R2 relaxometry permits rapid whole-liver iron quantification in a single breath-hold. An added benefit of the R2* relaxometry technique is that myocardial iron concentration can be simultaneously determined, either in 2 separate axial breath-hold acquisitions (liver and myocardium) or in a single acquisition by including both the myocardium and the liver in the sagittal slices.[61]

Sequence and Parameters

As mentioned earlier, accurate quantitative PDFF mapping requires a correction for T2* decay to account for iron in the liver. The dose-dependent signal decay due to iron can either be characterized by T2* (relaxation time, reported in msec) or its inverse R2* (relaxation rate, reported in sec^{-1}). The higher liver iron concentration results in faster signal decay, yielding shorter T2* and longer R2* values. Thus, the same multiecho

Table 2 Sample of Suggested Formulas for Converting R2* Values to Liver Iron Concentration (LIC)

Publication	Formula
Garbowski et al[62]	LIC = 0.032(R2*) − 0.14
Hankins et al[63]	LIC = 0.028(R2*) − 0.45
Henninger et al[64]	LIC = 0.024(R2*) − 0.277
Jhaveri et al[65]	LIC = 0.0266(R2*)
Wood et al[66]	LIC = 0.0254(R2*) + 0.202

GRE sequence used for PDFF mapping also provides a map of T2* (or equivalently, R2*), a surrogate for liver iron concentration. Typical parameters are listed in Table 1.

Interpretation Pearls

R2* maps are interpreted similarly to PDFF maps with the largest fit ROIs placed on the liver, avoiding large vessels (Fig. 1B). It is preferred to report an R2* value rather than T2*, as R2* has a positive linear correlation with liver iron concentration and is thus a more intuitive biomarker of iron overload.

Currently, the R2* value can be converted to a liver iron concentration based on technique specific formulas from the literature which where validated on 1.5T scanners against biopsy or R2 FerriScan® standards.[62-66] The formulas from these references are listed in Table 2. Although there are slight differences between the formulas, they provide similar results in the clinically meaningful liver iron concentration range and are unlikely to result in significant differences in patient management. The rate of signal decay is also affected by field strength, and Storey et al showed that the rate of decay is approximately twice as fast at 3T than 1.5T.[67] Thus, if the exam is performed at 3T, the above formulas should be adjusted accordingly to compensate for field strength effects.

Pitfalls

One of the most common causes of R2* mapping failure is severe iron overload. This is recognizable as a pixelated appearance of the R2* map in the liver, as neighboring pixels have spurious extreme (very low or very high) R2* values due to a curve fitting algorithm failure (Fig. 3). This is most pronounced when imaging at 3T when the signal decay is nearly twice as fast as at 1.5T, because the multiecho acquisition designed for PDFF estimation may not be fast enough to adequately sample the rapid signal decay. To minimize this risk, the sequence parameters can be modified to pack the echoes as early and tightly as possible. Protocols generally include a sub-millisecond first echo, but this may not be enough to overcome the rapid signal decay that occurs at very high iron levels. Scheduling patients who are suspected to have very high iron levels at 1.5T will likely decrease the number of failures. A suggested method of triaging would be to use a threshold serum ferritin level (eg, 600 ng/mL), at which patients would be directed to 1.5T.[68] R2 relaxometry or signal-intensity ratio can also be considered in patients with suspected very high liver iron concentration.

Liver Stiffness Measurement

Hepatic fibrosis and cirrhosis are the long-term consequences of untreated hepatic steatosis and hepatic iron overload. MR

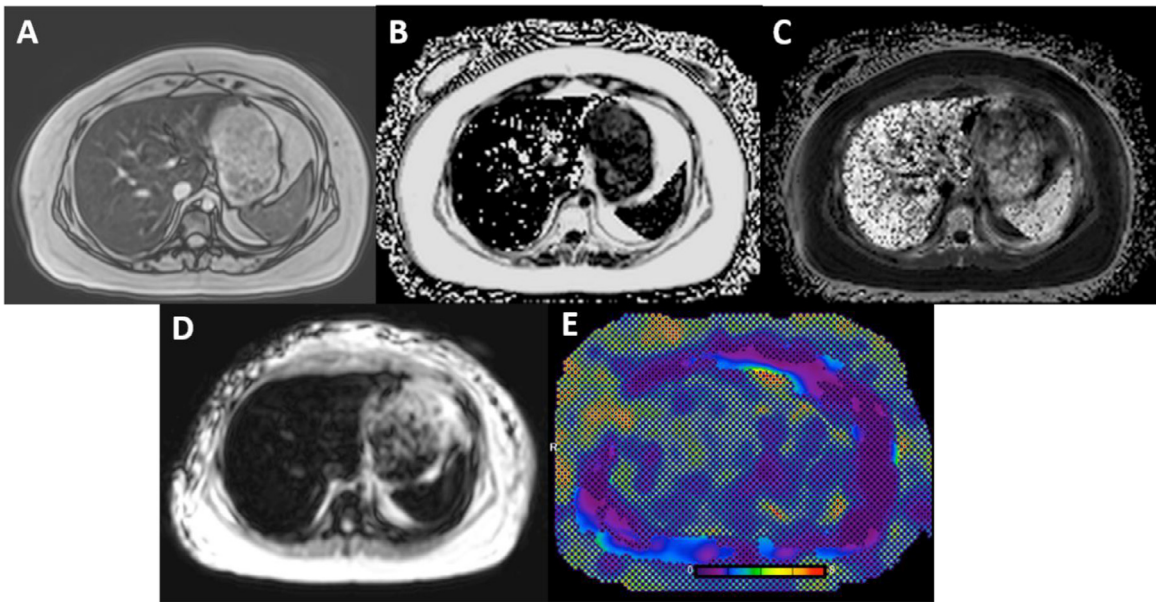

Figure 3 Metabolic MRI images of a young adult with sickle cell disease. T1-GRE with a TE of 2.4 msec (A) shows a markedly hypointense liver indicative of severe hepatic iron overload. The proton density fat-fraction map (B) and R2* map (C) both have a pixelated appearance indicative of a technical failure due to the severe iron overload. The MR elastography portion of the exam also failed due to the high iron levels as the liver is markedly hypointense on the magnitude image with a TE of 20 msec (D) and the entire color stiffness map (E) is cross-hatched.

elastography is an imaging technique which provides a non-invasive and safe alternative to biopsy for the assessment of hepatic fibrosis.[69,70] Early detection of hepatic fibrosis is crucial as proper treatment of the underlying cause can halt or possibly reverse the extent of fibrosis.[19,71,72]

An important additional population of young patients at risk for hepatic fibrosis is patients who have undergone a Fontan procedure for congenital heart disease and single ventricle physiology. The Fontan procedure redirects systemic venous blood to the lungs without passing through a ventricle.[73] Systemic venous hypertension as a result of Fontan circulation can cause increased hepatic sinusoidal pressures, chronic liver disease and fibrosis.[74] Preliminary evaluation using MR elastography has shown increased liver stiffness in Fontan patients proportional to duration of Fontan circulation.[75,76] However, ultrasound elastography data have correlated increased liver stiffness in the early post-operative period with increased Inferior vena cava pressure, suggesting that the early increase in liver stiffness postoperatively is due to venous congestion rather than fibrosis.[77] These findings may confound the use of elastography for fibrosis assessment in this population.

Corrected T1 mapping (cT1) of the liver (Fig. 4) is an alternative MRI technique that has been shown to detect hepatic inflammation and fibrosis in adults.[78] However, currently there is a paucity of data for this technique in children which limits its widespread clinical application in this population. With future validation, there is potential to use this technique as an alternative or adjunct to MR elastography. The main distinction is that corrected T1 mapping does not require additional equipment (described later) and it has the potential to differentiate simple steatosis (NAFL) from the more advanced steatohepatitis (NASH). Corrected T1 mapping is currently only available as a commercial product requiring offsite analysis at an additional cost (LiverMultiScan; Perspectum Diagnostics, Oxford, UK).

Equipment Setup, Sequence, and Parameters

MR elastography is a more technically involved process than conventional MR imaging because of the requirement for an external acoustic driver as the sound wave source. Figure 5 illustrates the typical MR elastography equipment configuration. Once the equipment is in place, a phase-contrast sequence with motion encoding gradients is synchronized with the acoustic waves generated by the external active driver and transmitted by the passive driver (paddle) into the liver as a mechanical shear wave. Image acquisition is most commonly performed at 4 axial planes through the mid liver of the largest cross-sectional area. The acquired phase images are transformed into wave images, which subsequently undergo automated post-processing and an inversion algorithm to yield an elastogram, or stiffness map, of the liver, reported in kilopascals (kPa).

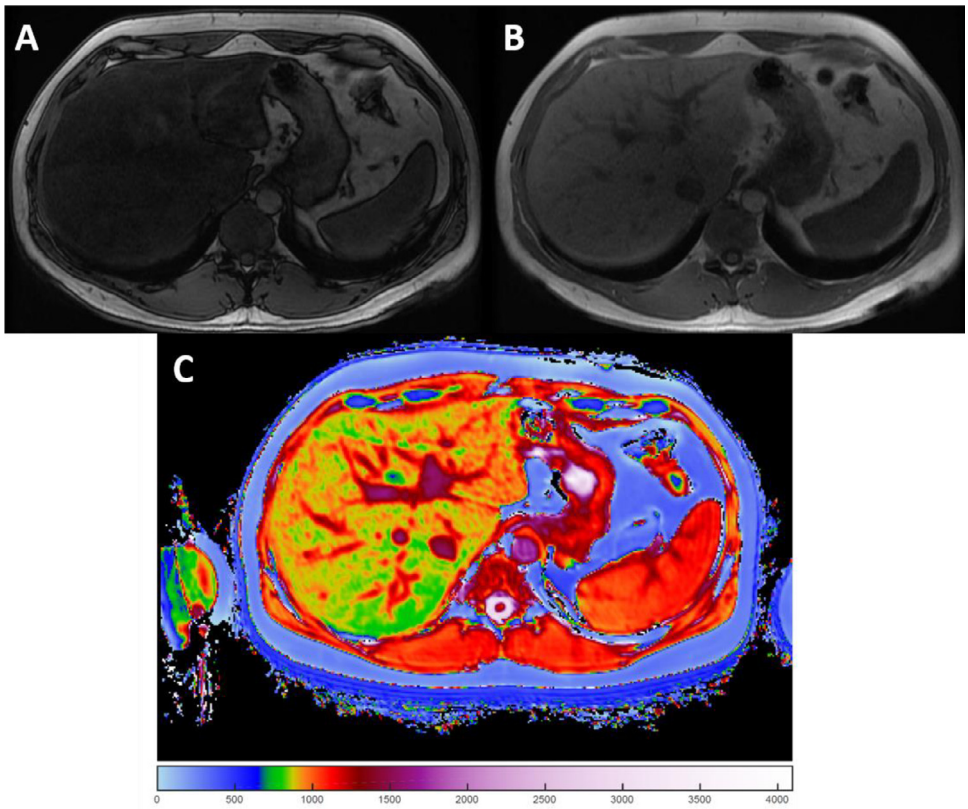

Figure 4 Corrected T1 MR imaging of hepatic inflammation and fibrosis. T1 opposed-phase (A) and in-phase (B) images of a young adult male demonstrate hepatic steatosis. The corresponding corrected T1 map (C) shows areas of superimposed hepatic inflammation and fibrosis (red and orange on the color map) indicative of steatohepatitis.

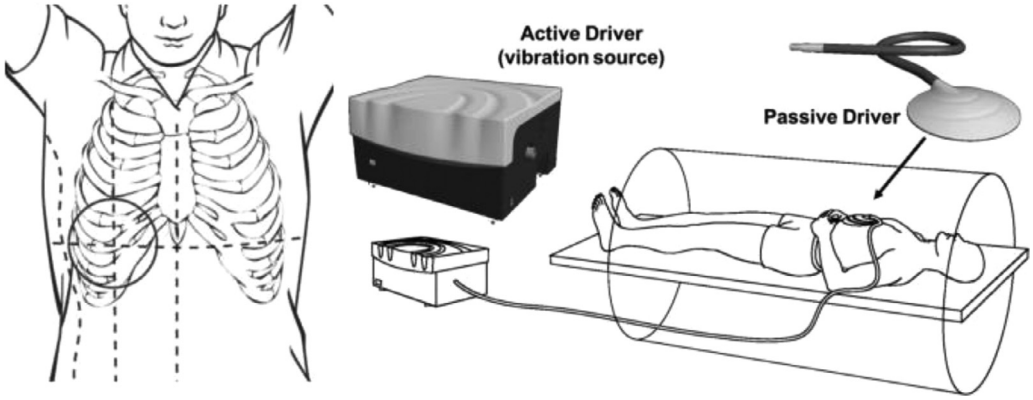

Figure 5 Schematic demonstrating elastography equipment and proper passive driver positioning over the right thoracoabdominal wall. Note the active driver is located in the control room and connected to the passive driver via a pneumatic tube. (Reprinted with permission from reference[92]).

Multiple key technical factors must be addressed to ensure a high-quality elastography exam.[79] First, the patient should be fasting for at least 4 hours. Postprandial increases in portal blood flow may result in transient increases in liver stiffness in patients with chronic liver disease.[80,81] It is also important to check proper connection of all hardware components (active driver, tubing, and passive driver) to ensure transmission of the acoustic vibrations from the active driver to the passive driver (eg, air leak from connectors or a kink in the tubing). The position of the passive driver is also critical. The passive driver should be placed over the right hepatic lobe, broadly contacting the right anterior body wall at the level of the xyphoid, and secured in place with the elastic straps underneath a phased array torso coil.[82-84] It is important not to position the passive driver too high or too low, as intervening lung or colon will interfere with wave propagation. In most cases, the driver frequency should be set to 60 Hz, as this setting was used in most reference studies. The driver amplitude is adjustable and should be set according to the patient's weight and body habitus, with suggested values of 25% for thin or very young (<1-year-old) patients, 50% for standard patients and 75% for larger patients.[69,79,85]

The phase-contrast sequence is most commonly implemented using a 2D gradient recalled echo (GRE), but 2D spin-echo echo-planar imaging (SE-EPI) pulse sequence is emerging. GRE-based MR elastography (MRE) sequence was introduced first and had been used more extensively in the clinical validation studies.[86-88] One potential advantage of the SE-EPI over GRE based MRE sequence is its faster readout and acquisition times, allowing acquisition of all 4 slices in a single breath hold, and relative robustness in patients with iron overload. A recent comparison of GRE and SE-EPI MRE in pediatric patients found high agreement in stiffness values between the 2 sequences, with reduced respiratory motion artifacts with the SE-EPI sequence.[89] When using GRE-based MRE, it is important to choose an in-phase TE to minimize the signal loss from steatosis. Typical sequence parameters for GRE-based MRE are listed in Table 3.

Each 2D slice typically involves a separate breath hold acquisition (particularly using the GRE technique). The acquisition time using standard parameters is approximately 15 seconds per slice. Ideally, imaging is performed at the same phase of respiration as when the passive driver was secured (ie, place the passive driver on at end-expiration and perform all imaging at end-expiration).

Interpretation Pearls

After the image acquisition, there are multiple output images including the magnitude, phase, and wave images. These can be used to assure quality control. However, the liver stiffness measurement is performed on the quantitative elastogram. The post-processed elastogram includes overlying hatch marks depicting the 95% confidence map. Large ROIs placed on the liver in the areas not covered by the 95% confidence map will yield a liver stiffness measurement in kPa. The average of these ROIs across the 4 sections should be reported, using a weighted mean based on ROI size.

Table 3 Summary of Standard Pulse Sequence Parameters for GRE-Based MR Elastography on 1.5T and 3T Clinical Scanners

Parameter/Field strength	1.5T[85]	3T[86,88]
Matrix	256 × 64	256 × 64
NEX	1	1
TE (ms)	20	20.2
TR (ms)	48	50
Bandwidth	32	31.25
Flip angle (degrees)	25	30
Number of slices	4	4
Slice thickness (mm/gap)	8/2.5	10/10
Number of phases	4	4
MEG frequency (Hz)	60	
Axis of MEG	z	z
Driver frequency	60	
Driver cycles/trigger	3	
Number of breath-holds	4	4
Acceleration factor	2	2
Scan time per breath hold	~15 sec	~16 sec

Although the majority of the validation data for MR elastography was performed in adults, a few studies have established threshold stiffness values for children. A large dual center study established 2.69-2.77 kPa (provided as a range due to varying methods of analysis) as the threshold for differentiating no fibrosis (stage 0) from any fibrosis (stage $\geq$ 1) and 3.03-3.33 kPa as the threshold for advanced fibrosis (stage $\geq$3).[86] Another case series established a threshold of 2.71 kPa for stage 2 or greater fibrosis.[87] The most recent series demonstrated 2.45 kPa as the mean liver stiffness in a series of 81 healthy children.[88]

Pitfalls

The added equipment required for MR elastography provides an additional opportunity for technical failures. One of the most common causes of an equipment related failure is a kinked or disconnected tube between the active and passive drivers. This results in a nondiagnostic elastogram as no waves can reach the liver. Body habitus also plays a role in the elastogram image quality. As we mentioned earlier, the driver amplitude can be increased to accommodate larger patients, but too much soft-tissue interposed between the passive driver and the liver surface will dampen the shear wave delivery to the liver and result in a poor quality elastogram. In addition, improper positioning of the passive driver on the patient can lead to poor wave propagation that is reflected in poor elastogram maps at deeper levels in the liver (Fig. 6). This can be a problem for young children in which the driver can slide as the anterior coil is place on the patient. In these cases, it can be helpful to tape a Vitamin E capsule or other marker on the passive driver to make its position visible on the localizer images.

As with any breath-hold imaging of the liver, respiratory motion artifact will degrade image quality and result in a poor quality elastogram. A recent study comparing MR elastography acquisition techniques using a GRE sequence showed that either acquiring all 4 slices continuously without respiratory suspension (52 second total acquisition) or acquiring as 4 short breath holds (8.9 seconds) using sparse sampling and compressed sensing reconstruction, yielded comparable image quality and stiffness values to the standard 4 breath hold (13.3 seconds each) acquisition.[90] Newer acceleration techniques may lead to shorter MR elastography sequences without requirement for breath holding.

Lastly, patients with iron overload (eg, T2* < 10 msec; R2* > 100/s) may have poor quality or nondiagnostic elastograms due to iron related signal loss on the GRE sequence which is typically acquired at TE$\sim$20 msec.[91] SE-EPI sequences are becoming available and will help in this situation as spin echo sequences are less susceptible to iron overload.

Conclusion

Metabolic liver MRI quantification of liver fat, iron, and fibrosis is increasingly utilized in pediatric patients and is an important noninvasive tool in the management of pediatric patients with chronic liver diseases. Understanding the nuances of metabolic liver MRI interpretation, as well as

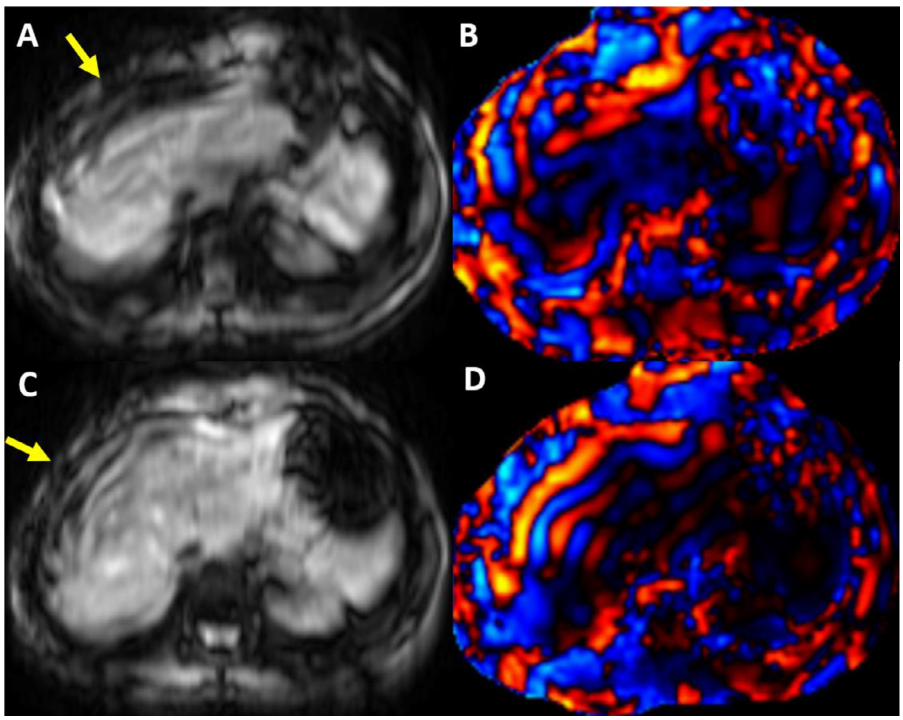

Figure 6 MR elastogram images of an 11-year-old female. The initial magnitude image (A) shows the driver placed anteriorly (arrow) with poor wave organization and propagation on the corresponding wave map (B). The sequence was repeated after moving the driver more laterally. The subsequent magnitude image (C) shows the driver positioned more laterally (arrow) with better wave propagation through the liver on the corresponding wave map (D).

Table 4 Summary of Pearls and Pitfalls in Metabolic Liver MRI in Pediatric Patients

Pearls	Pitfalls
Draw large ROIs, sampling as much of the liver as possible, but taking care to avoid major vessels.	Motion artifacts, particularly from respiration, can degrade quantitative assessment. Newer motion-robust sequences are in clinical development and may help minimize this.
Consider using serum ferritin levels to triage patients to 1.5T scanners to avoid R2* mapping failures.	R2* relaxometry can fail in the setting of extremely high liver iron concentration. Consider shortening initial TE and inter-echo interval to < 1 msec, or alternatively R2 relaxometry or signal-intensity ratio methods in these cases.
If MR elastography stiffness maps are poor-quality or nondiagnostic, evaluate the source magnitude and phase images to see if the shear wave motion is visible.	MR elastography can fail in the setting of hepatic iron overload. Use of SE-EPI sequences will increase likelihood of a diagnostic quality exam.
If the motion is absent or less than expected, ensure the active driver is turned on, passive driver is properly positioned, and driver tubing is properly connected.	Ultrasound shear-wave elastography technique may be indicated in whom MR elastography is nondiagnostic due to iron overload, as ultrasound is not affected by presence of iron.
Check the R2* map if the MR elastography failure is related to iron overload.	
Corrected T1 mapping has not yet been validated in pediatric patients but may be an alternative to MR elastography for liver fibrosis assessment without the need for acoustic driver hardware	In the setting of fat-water swap, PDFF and R2* data is not reliable.
	In the setting of severe iron overload, PDFF data may not be reliable.

anticipating potential problems with image acquisition and map generation in pediatric patients, will benefit pediatric radiologists applying these techniques to children. Table 4 provides a summary of the pearls and pitfalls of metabolic liver MRI described in this article.

References

1. Lavine JE, Schwimmer JB: Nonalcoholic fatty liver disease in the pediatric population. Clin Liver Di 8. https://doi.org/10.1016/j.cld.2004.04.010, 2004. 549–58, viii–ix
2. Nobili V, Alisi A, Valenti L, et al: NAFLD in children: New genes, new diagnostic modalities and new drugs. Nat Rev Gastroenterol Hepatol 16:517-530, 2019. https://doi.org/10.1038/s41575-019-0169-z
3. Eckel RH, Grundy SM, Zimmet PZ. The metabolic syndrome. Lancet. 2005 Apr 16-22;365(9468):1415-28. https://doi.org/10.1016/S0140-6736(05)66378-7.
4. Zimmet P, Alberti G, Kaufman F, et al: The metabolic syndrome in children and adolescents. Lancet 369:2059-2061, 2007. https://doi.org/10.1016/S0140-6736(07)60958-1
5. Schwimmer JB, Zepeda A, Newton KP, et al: Longitudinal assessment of high blood pressure in children with nonalcoholic fatty liver disease. PLoS One 9. https://doi.org/10.1371/journal.pone.0112569, 2014
6. Schwimmer JB, Pardee PE, Lavine JE, et al: Cardiovascular risk factors and the metabolic syndrome in pediatric nonalcoholic fatty liver disease. Circulation 118:277-283, 2008. https://doi.org/10.1161/CIRCULATIONAHA.107.739920
7. Angelucci E, Brittenham GM, McLaren CE, et al: Hepatic iron concentration and total body iron stores in thalassemia major. N Engl J Med 343:327-331, 2000. https://doi.org/10.1056/NEJM200008033430503
8. Olivieri NF, Brittenham GM: Iron-chelating therapy and the treatment of thalassemia. Blood 89:739-761, 1997. https://doi.org/10.1182/blood.v89.3.739
9. Porter JB, Garbowski M: The pathophysiology of transfusional iron overload. Hematol Oncol Clin North Am 28:683-701, 2014. https://doi.org/10.1016/j.hoc.2014.04.003
10. Italian Working Group on Endocrine Complications in Non-endocrine Diseases: Multicentre study on prevalence of endocrine complications in thalassaemia major. Clin Endocrinol (Oxf). 42:581-586, 1995. Available at: http://www.ncbi.nlm.nih.gov/pubmed/7634497. Accessed January 6, 2020
11. Caussy C, Reeder SB, Sirlin CB, et al: Noninvasive, quantitative assessment of liver fat by MRI-PDFF as an endpoint in NASH Trials. Hepatology 68:763-772, 2018. https://doi.org/10.1002/hep.29797
12. Caussy C, Brissot J, Singh S, et al: Prospective, same-day, direct comparison of CAP with the M vs the XL probe in patients with nonalcoholic fatty liver disease, using magnetic resonance imaging proton density fat fraction as the standard. Clin Gastroenterol Hepatol 2019. https://doi.org/10.1016/j.cgh.2019.11.060
13. Ajmera VH, Cachay E, Ramers C, et al: MRI assessment of treatment response in HIV-associated NAFLD: A randomized trial of a stearoyl-coenzyme-A-desaturase-1 inhibitor (ARRIVE Trial). Hepatology 70:1531-1545, 2019. https://doi.org/10.1002/hep.30674
14. Wood JC, Zhang P, Rienhoff H, et al: R2 and R2* are equally effective in evaluating chronic response to iron chelation. Am J Hematol 89:505-508, 2014. https://doi.org/10.1002/ajh.23673
15. Cancado R, Watman NP, Lobo C, et al: Assessment of liver and cardiac iron overload using MRI in patients with chronic anemias in Latin American countries: results from ASIMILA study. Hematology 23:676-682, 2018. https://doi.org/10.1080/10245332.2018.1461292
16. França M, Martí-Bonmatí L, Silva S, et al: Optimizing the management of hereditary haemochromatosis: the value of MRI R2* quantification to predict and monitor body iron stores. Br J Haematol 183:491-493, 2018. https://doi.org/10.1111/bjh.14982
17. Lemoinne S, Friedman SL: New and emerging anti-fibrotic therapeutics entering or already in clinical trials in chronic liver diseases. Curr Opin Pharmacol 49:60-70, 2019. https://doi.org/10.1016/j.coph.2019.09.006
18. Yoon YJ, Friedman SL, Lee YA: Antifibrotic therapies: Where are we now? Semin Liver Dis 36:87-98, 2016. https://doi.org/10.1055/s-0036-1571295
19. Friedman SL: Evolving challenges in hepatic fibrosis. Nat Rev Gastroenterol Hepatol 7:425-436, 2010. https://doi.org/10.1038/nrgastro.2010.97
20. Younossi ZM, Gramlich T, Yao CL, et al: Nonalcoholic fatty liver disease: Assessment of variability in pathologic interpretations. Mod Pathol 11:560-565, 1998
21. Ratziu V, Charlotte F, Heurtier A, et al: Sampling variability of liver biopsy in nonalcoholic fatty liver disease. Gastroenterology 128:1898-1906, 2005. https://doi.org/10.1053/j.gastro.2005.03.084
22. Bravo AA, Sheth SG, Chopra S: Liver biopsy. N Engl J Med 344:495-500, 2001. https://doi.org/10.1056/NEJM200102153440706

23. Rockey DC, Caldwell SH, Goodman ZD, et al: Liver biopsy. Hepatology 49:1017-1044, 2009. https://doi.org/10.1002/hep.22742
24. Gilmore IT, Burroughs A, Murray-Lyon IM, et al: Indications, methods, and outcomes of percutaneous liver biopsy in England and Wales: An audit by the British Society of Gastroenterology and the Royal College of Physicians of London. Gut 36:437-441, 1995. https://doi.org/10.1136/gut.36.3.437
25. Cadranel JF, Rufat P, Degos F: Practices of liver biopsy in France: Results of a prospective nationwide survey. Hepatology 32:477-481, 2000. https://doi.org/10.1053/jhep.2000.16602
26. McGill DB, Rakela J, Zinsmeister AR, et al: A 21-year experience with major hemorrhage after percutaneous liver biopsy. Gastroenterology 99:1396-1400, 1990. https://doi.org/10.1016/0016-5085(90)91167-5
27. Brunt EM: Pathology of nonalcoholic fatty liver disease. Nat Rev Gastroenterol Hepatol 7:195-203, 2010. https://doi.org/10.1038/nrgastro.2010.21
28. Brunt EM, Tiniakos DG: Pathology of steatohepatitis. Bailliere's Best Pract Res Clin Gastroenterol 16:691-707, 2002. https://doi.org/10.1053/bega.2002.0326
29. Levene AP, Goldin RD: The epidemiology, pathogenesis and histopathology of fatty liver disease. Histopathology 61:141-152, 2012. https://doi.org/10.1111/j.1365-2559.2011.04145.x
30. Kühn J-P, Jahn C, Hernando D, et al: T1 bias in chemical shift-encoded liver fat-fraction: Role of the flip angle. J Magn Reson Imaging 40:875-883, 2014. https://doi.org/10.1002/jmri.24457
31. Bottomley PA, Foster TH, Argersinger RE, et al: A review of normal tissue hydrogen NMR relaxation times and relaxation mechanisms from 1-100 MHz: Dependence on tissue type, NMR frequency, temperature, species, excision, and age. Med Phys 11:425-448, 1984. https://doi.org/10.1118/1.595535
32. Blüml S, Schad LR, Stepanow B, et al: Spin−lattice relaxation time measurement by means of a TurboFLASH technique. Magn Reson Med 30:289-295, 1993. https://doi.org/10.1002/mrm.1910300304
33. Labranche R, Gilbert G, Cerny M, et al: Liver iron quantification with MR imaging: A primer for radiologists. Radiographics 38:392-412, 2018. https://doi.org/10.1148/rg.2018170079
34. Reeder SB, Bice EK, Yu H, et al: On the performance of T2 * correction methods for quantification of hepatic fat content. Magn Reson Med 67:389-404, 2012. https://doi.org/10.1002/mrm.23016
35. Hamilton G, Yokoo T, Bydder M, et al: In vivo characterization of the liver fat 1H MR spectrum. NMR Biomed 24:784-790, 2011. https://doi.org/10.1002/nbm.1622
36. Reeder SB, Robson PM, Yu H, et al: Quantification of hepatic steatosis with MRI: The effects of accurate fat spectral modeling. J Magn Reson Imaging. 29:1332-1339, 2009. https://doi.org/10.1002/jmri.21751
37. Middleton MS, Van Natta ML, Heba ER, et al: Diagnostic accuracy of magnetic resonance imaging hepatic proton density fat fraction in pediatric nonalcoholic fatty liver disease. Hepatology 67:858-872, 2018. https://doi.org/10.1002/hep.29596
38. Haufe WM, Wolfson T, Hooker CA, et al: Accuracy of PDFF estimation by magnitude-based and complex-based MRI in children with MR spectroscopy as a reference. J. Magn Reson Imaging 46:1641-1647, 2017. https://doi.org/10.1002/jmri.25699
39. Szczepaniak LS, Nurenberg P, Leonard D, et al: Magnetic resonance spectroscopy to measure hepatic triglyceride content: Prevalence of hepatic steatosis in the general population. Am J Physiol Endocrinol Metab 288:E462-E468, 2005. Available at http://ajpendo.physiology.org/cgi/doi/10.1152/ajpendo.00064.2004. Accessed April 30, 2017
40. Szczepaniak LS, Babcock EE, Schick F, et al: Measurement of intracellular triglyceride stores by 1H spectroscopy: Validation in vivo. Am J Physiol Endocrinol Metab 276. https://doi.org/10.1152/ajpendo.1999.276.5.e977, 1999
41. Thomsen C, Becker U, Winkler K, et al: Quantification of liver fat using magnetic resonance spectroscopy. Magn Reson Imaging. 12:487-495, 1994. https://doi.org/10.1016/0730-725x(94)92543-7
42. Longo R, Ricci C, Masutti F, et al: Fatty infiltration of the liver. Quantification by 1H localized magnetic resonance spectroscopy and comparison with computed tomography. Invest Radiol 28:297-302, 1993. Available at: http://www.ncbi.nlm.nih.gov/pubmed/8478169. Accessed December 19, 2019
43. Longo R, Pollesello P, Ricci C, et al: Proton MR spectroscopy in quantitative in vivo determination of fat content in human liver steatosis. J Magn Reson Imaging 5:281-285, 1995. https://doi.org/10.1002/jmri.1880050311
44. Yokoo T, Shiehmorteza M, Hamilton G, et al: Estimation of hepatic proton-density fat fraction by using MR imaging at 3.0 T. Radiology 258:749-759, 2011. https://doi.org/10.1148/radiol.10100659
45. Yokoo T, Bydder M, Hamilton G, et al: Nonalcoholic fatty liver disease: Diagnostic and fat-grading accuracy of low-flip-angle multiecho gradient-recalled-echo MR imaging at 1.5 T. Radiology 251:67-76, 2009. https://doi.org/10.1148/radiol.2511080666
46. Meisamy S, Hines CDG, Hamilton G, et al: Quantification of hepatic steatosis with T1-independent, T2*-corrected MR imaging with spectral modeling of fat: Blinded comparison with MR spectroscopy. Radiology 258:767-775, 2011. https://doi.org/10.1148/radiol.10100708
47. Bashir MR, Zhong X, Nickel MD, et al: Quantification of hepatic steatosis with a multistep adaptive fitting MRI approach: Prospective validation against MR spectroscopy. Am J Roentgenol 204:297-306, 2015. https://doi.org/10.2214/AJR.14.12457
48. Campo CA, Hernando D, Schubert T, et al: Standardized approach for ROI-based measurements of proton density fat fraction and R2* in the liver. Am J Roentgenol 209:592-603, 2017. https://doi.org/10.2214/AJR.17.17812
49. Jaimes C, Gee MS: Strategies to minimize sedation in pediatric body magnetic resonance imaging. Pediatr Radiol 46:916-927, 2016. https://doi.org/10.1007/s00247-016-3613-z
50. Gilligan LA, Dillman JR, Tkach JA, et al: Comparison of navigator-gated and breath-held image acquisition techniques for multi-echo quantitative dixon imaging of the liver in children and young adults. Abdom Radiol (New York) 44:2172-2181, 2019. https://doi.org/10.1007/s00261-019-01960-1
51. Jaimes C, Kirsch JE, Gee MS: Fast, free-breathing and motion-minimized techniques for pediatric body magnetic resonance imaging. Pediatr Radiol 48:1197-1208, 2018. https://doi.org/10.1007/s00247-018-4116-x
52. Armstrong T, Dregely I, Stemmer A, et al: Free-breathing liver fat quantification using a multiecho 3D stack-of-radial technique. Magn Reson Med 79:370-382, 2018. https://doi.org/10.1002/mrm.26693
53. Pooler BD, Hernando D, Ruby JA, et al: Validation of a motion-robust 2D sequential technique for quantification of hepatic proton density fat fraction during free breathing. J Magn Reson Imaging 48:1578-1585, 2018. https://doi.org/10.1002/jmri.26056
54. Jehn M, Clark JM, Guallar E: Serum ferritin and risk of the metabolic syndrome in U.S. adults. Diabetes Care 27:2422-2428, 2004. https://doi.org/10.2337/diacare.27.10.2422
55. Bozzini C, Girelli D, Olivieri O, et al: Prevalence of body iron excess in the metabolic syndrome. Diabetes Care 28:2061-2063, 2005. https://doi.org/10.2337/diacare.28.8.2061
56. Wrede CE, Buettner R, Bollheimer LC, et al: Association between serum ferritin and the insulin resistance syndrome in a representative population. Eur J Endocrinol 154:333-340, 2006. https://doi.org/10.1530/eje.1.02083
57. Kim CH, Kim HK, Bae SJ, et al: Association of elevated serum ferritin concentration with insulin resistance and impaired glucose metabolism in Korean men and women. Metabolism 60:414-420, 2011. https://doi.org/10.1016/j.metabol.2010.03.007
58. Moris W, Verhaegh P, Jonkers D, et al: Hyperferritinemia in nonalcoholic fatty liver disease: Iron accumulation or inflammation? Semin Liver Dis 39:476-482, 2019. https://doi.org/10.1055/s-0039-1693114
59. Dongiovanni P, Fracanzani AL, Fargion S, et al: Iron in fatty liver and in the metabolic syndrome: A promising therapeutic target. J Hepatol 55:920-932, 2011. https://doi.org/10.1016/j.jhep.2011.05.008
60. Tsitsikas DA, Nzouakou R, Ameen V, et al: Comparison of serial serum ferritin measurements and liver iron concentration assessed by MRI in adult transfused patients with sickle cell disease. Eur J Haematol 92:164-167, 2014. https://doi.org/10.1111/ejh.12230

61. Serai SD, Trout AT, Fleck RJ, et al: Measuring liver T2* and cardiac T2* in a single acquisition. Abdom Radiol (New York) 43:2303-2308, 2018. https://doi.org/10.1007/s00261-018-1477-4
62. Garbowski MW, Carpenter JP, Smith G, et al: Biopsy-based calibration of T2* magnetic resonance for estimation of liver iron concentration and comparison with R2 Ferriscan. J Cardiovasc Magn Reson 16. https://doi.org/10.1186/1532-429X-16-40, 2014
63. Hankins JS, McCarville MB, Loeffler RB, et al: R2* magnetic resonance imaging of the liver in patients with iron overload. Blood 113:4853-4855, 2009. https://doi.org/10.1182/blood-2008-12-191643
64. Henninger B, Zoller H, Rauch S, et al: R2∗ relaxometry for the quantification of hepatic iron overload: Biopsy-based calibration and comparison with the literature. RoFo Fortschritte Auf Dem Gebiet Der Rontgenstrahlen Und Der Bildgeb. Verfahren 187:472-479, 2015. https://doi.org/10.1055/s-0034-1399318
65. Jhaveri KS, Kannengiesser SAR, Ward R, et al: Prospective evaluation of an R2* method for assessing liver iron concentration (LIC) against FerriScan: Derivation of the calibration curve and characterization of the nature and source of uncertainty in the relationship. J Magn Reson Imaging 49:1467-1474, 2019. https://doi.org/10.1002/jmri.26313
66. Wood JC, Enriquez C, Ghugre N, et al: MRI R2 and R2* mapping accurately estimates hepatic iron concentration in transfusion-dependent thalassemia and sickle cell disease patients. Blood 106:1460-1465, 2005. https://doi.org/10.1182/blood-2004-10-3982
67. Storey P, Thompson AA, Carqueville CL, et al: R2* imaging of transfusional iron burden at 3T and comparison with 1.5T. J Magn Reson Imaging 25:540-547, 2007. https://doi.org/10.1002/jmri.20816
68. Yokoo T, Pedrosa I, Hernando D, et al: Bayesian selection of dedicated liver iron quantification MRI for patients with clinically-significant iron overload. In: ISMRM, Montreal, Canada, 2019; Montreal, Canada.
69. Binkovitz LA, El-Youssef M, Glaser KJ, et al: Pediatric MR elastography of hepatic fibrosis: Principles, technique and early clinical experience. Pediatr Radiol 42:402-409, 2012. https://doi.org/10.1007/s00247-011-2298-6
70. Serai SD, Towbin AJ, Podberesky DJ: Pediatric liver MR elastography. Dig Dis Sci 57:2713-2719, 2012. https://doi.org/10.1007/s10620-012-2196-2
71. Friedman SL: Hepatic fibrosis-Overview. Toxicology 254:120-129, 2008. https://doi.org/10.1016/j.tox.2008.06.013
72. Bortolotti F, Guido M: Reversal of liver cirrhosis: A desirable clinical outcome and its pathogenic background. J Pediatr Gastroenterol Nutr 44:401-406, 2007. https://doi.org/10.1097/MPG.0b013e318032069a
73. Fredenburg TB, Johnson TR, Cohen MD: The Fontan procedure: Anatomy, complications, and manifestations of failure. RadioGraphics 31:453-463, 2011. https://doi.org/10.1148/rg.312105027
74. Gordon-Walker TT, Bove K, Veldtman G: Fontan-associated liver disease: A review. J Cardiol 74:223-232, 2019. https://doi.org/10.1016/j.jjcc.2019.02.016
75. Wallihan DB, Podberesky DJ, Marino BS, et al: Relationship of MR elastography determined liver stiffness with cardiac function after Fontan palliation. J Magn Reson Imaging 40:1328-1335, 2014. https://doi.org/10.1002/jmri.24496
76. Serai SD, Wallihan DB, Venkatesh SK, et al: Magnetic resonance elastography of the liver in patients status-post fontan procedure: Feasibility and preliminary results. Congenit Heart Dis 9:7-14, 2014. https://doi.org/10.1111/chd.12144
77. DiPaola FW, Schumacher KR, Goldberg CS, et al: Effect of Fontan operation on liver stiffness in children with single ventricle physiology. Eur Radiol 27:2434-2442, 2017. https://doi.org/10.1007/s00330-016-4614-x
78. Banerjee R, Pavlides M, Tunnicliffe EM, et al: Multiparametric magnetic resonance for the non-invasive diagnosis of liver disease. J Hepatol 60:69-77, 2014. https://doi.org/10.1016/j.jhep.2013.09.002
79. Guglielmo FF, Venkatesh SK, Mitchell DG: Liver MR elastography technique and image interpretation: Pearls and pitfalls. Radiographics 39:1983-2002, 2019. https://doi.org/10.1148/rg.2019190034
80. Yin M, Talwalkar JA, Glaser KJ, et al: Dynamic postprandial hepatic stiffness augmentation assessed with MR elastography in patients with chronic liver disease. Am J Roentgenol 197:64-70, 2011. https://doi.org/10.2214/AJR.10.5989
81. Mederacke I, Wursthorn K, Kirschner J, et al: Food intake increases liver stiffness in patients with chronic or resolved hepatitis C virus infection. Liver Int 29:1500-1506, 2009. https://doi.org/10.1111/j.1478-3231.2009.02100.x
82. Venkatesh SK, Yin M, Glockner JF, et al: MR elastography of liver tumors: Preliminary results. Am J Roentgenol 190:1534-1540, 2008. https://doi.org/10.2214/AJR.07.3123
83. Venkatesh SK, Wang G, Lim SG, et al: Magnetic resonance elastography for the detection and staging of liver fibrosis in chronic hepatitis B. Eur Radiol 24:70-78, 2014. https://doi.org/10.1007/s00330-013-2978-8
84. Venkatesh SK, Yin M, Takahashi N, et al: Non-invasive detection of liver fibrosis: MR imaging features vs. MR elastography. Abdom Imaging 40:766-775, 2015. https://doi.org/10.1007/s00261-015-0347-6
85. Joshi M, Dillman JR, Towbin AJ, et al: MR elastography: High rate of technical success in pediatric and young adult patients. Pediatr Radiol 47:838-843, 2017. https://doi.org/10.1007/s00247-017-3831-z
86. Schwimmer JB, Behling C, Eduardo Angeles J, et al: Magnetic resonance elastography measured shear stiffness as a biomarker of fibrosis in pediatric nonalcoholic fatty liver disease HHS public access. Hepatology 66:1474-1485, 2017. https://doi.org/10.1002/hep.29241
87. Xanthakos SA, Podberesky DJ, Serai SD, et al: Use of magnetic resonance elastography to assess hepatic fibrosis in children with chronic liver disease. J Pediatr 164:186-188, 2014. https://doi.org/10.1016/j.jpeds.2013.07.050
88. Sawh MC, Newton KP, Goyal NP, et al: Normal range for MR elastography measured liver stiffness in children without liver disease. J Magn Reson Imaging 2019. https://doi.org/10.1002/jmri.26905. jmri.26905
89. Serai SD, Dillman JR, Trout AT: Spin-echo echo-planar imaging MR elastography versus gradient-echo MR elastography for assessment of liver stiffness in children and young adults suspected of having liver disease. Radiology 282:761-770, 2017. https://doi.org/10.1148/radiol.2016160589
90. Morin CE, Dillman JR, Serai SD, et al: Comparison of standard breath-held, free-breathing, and compressed sensing 2D gradient-recalled echo MR elastography techniques for evaluating liver stiffness. Am J Roentgenol 211:W279-W287, 2018. https://doi.org/10.2214/AJR.18.19761
91. Felker ER, Choi K-S, Sung K, et al: Liver MR elastography at 3 T: Agreement across pulse sequences and effect of liver R2* on image quality. AJR Am J Roentgenol 211:588-594, 2018. https://doi.org/10.2214/AJR.17.19288
92. RSNA Quantitative Imaging Biomarkers Alliance. Magnetic Resonance elastography of the liver: Stage 2—Consensus profile., 2018. Available at:https://qibawiki.rsna.org/images/a/a5/MRE-QIBAProfile-2018-05-02-CONSENSUS.pdf (Accessed December 27, 2019).